



A hidden structural variation in a known IRD gene: a cautionary tale of two new disease candidate genes

Hilary A. Scott,^{1,3} Anna Larson,^{1,3} Shi Song Rong,¹ Sudeep Mehrotra,¹ Rossano Butcher,¹ Katherine R. Chao,² Janey L. Wiggs,¹ Emily M. Place,¹ Eric A. Pierce,¹ and Kinga M. Bujakowska¹

¹Ocular Genomics Institute, Department of Ophthalmology, Massachusetts Eye and Ear, Harvard Medical School, Boston, Massachusetts 02115, USA; ²Center for Mendelian Genetics, Broad Institute of MIT and Harvard, Cambridge, Massachusetts 02142, USA

Abstract Rod-cone dystrophy (RCD), also known as retinitis pigmentosa, is an inherited condition leading to vision loss, affecting 1 in 3500 people. More than 270 genes are known to be implicated in the inherited retinal degenerations (IRDs), yet genetic diagnosis for ~30% of IRD of patients remains elusive despite advances in sequencing technologies. The goal of this study was to determine the genetic causality in a family with RCD. Family members were given a full ophthalmic exam at the Retinal Service at Massachusetts Eye and Ear and consented to genetic testing. Whole-exome sequencing (WES) was performed and variants of interest were Sanger-validated. Functional assays were conducted in zebrafish along with splicing assays in relevant cell lines to determine the impact on retinal function. WES identified variants in two potential candidate genes that segregated with disease: *GNL3* (G Protein Nucleolar 3) c.1187 + 3A > C and c.1568-8C > A; and *PDE4DIP* (Phosphodiester 4D Interacting Protein) c.3868G > A (p.Glu1290Lys) and c.4603G > A (p.Ala1535Thr). Both genes were promising candidates based on their retinal involvement (development and interactions with IRD-associated proteins); however, the functional assays did not validate either gene. Subsequent WES reanalysis with an updated bioinformatics pipeline and widened search parameters led to the detection of a 94-bp duplication in *PRPF31* (pre-mRNA Processing Factor 31) c.73_266dup (p.Asp56GlyfsTer33) as the causal variant. Our study demonstrates the importance of thorough functional characterization of new disease candidate genes and the value of reanalyzing next-generation sequencing sequence data, which in our case led to identification of a hidden pathogenic variant in a known IRD gene.

Corresponding author:
kinga_bujakowska@meei.harvard.edu

© 2022 Scott et al. This article is distributed under the terms of the Creative Commons Attribution-NonCommercial License, which permits reuse and redistribution, except for commercial purposes, provided that the original author and source are credited.

Ontology terms: peripheral visual field loss; progressive retinal degeneration

Published by Cold Spring Harbor Laboratory Press

doi:10.1101/mcs.a006131

[Supplemental material is available for this article.]

INTRODUCTION

Rod-cone degeneration (RCD) also known as retinitis pigmentosa (RP) is the most prevalent type of inherited retinal disease (IRD) which causes progressive vision loss affecting 1 in 3500 people worldwide (Haim 2002). IRDs can be inherited as autosomal recessive, autosomal dominant, Chromosome X-linked, and mitochondrial traits. Genetic diagnosis may additionally be complicated because of the genetic heterogeneity of IRDs with a wide spectrum of clinical phenotypes attributed to pathogenic variants in more than 270 genes (RetNet—

³These authors contributed equally to this work.

Retinal Information Network; uth.edu). Targeted exome panels that include known IRD genes as well as whole-exome sequencing are the standard approach for determining genetic diagnosis. These are largely focused on identifying single-nucleotide variants (SNVs), small indels, and increasingly large copy-number variations, allowing for the identification of causal mutations in ~60% of cases (Consugar et al. 2014; Carss et al. 2017; Ellingford et al. 2018). Current gene-based therapies require accurate molecular diagnosis, which provides an important incentive for determining the cause of disease in the remaining patients (Bainbridge et al. 2008; Maguire et al. 2008; MacLaren et al. 2014). A potential source of this missing causality could be found in novel candidate IRD genes, although rare, new IRD disease genes have been discovered within the last few years (e.g., *ARSG*, *CLCC1*, *POMGNT1*, *REEP6*, *AHR*, *IFT172*) (Bujakowska et al. 2015; Arno et al. 2016; Xu et al. 2016; Khateb et al. 2018; Li et al. 2018; Zhou et al. 2018). Cosegregation of the variant with the ocular phenotype in large pedigrees is often the only indicator of a novel gene initially. To classify the variant as causal, first a gene-disease association must be established, which requires further genetic and experimental investigation. Candidate genes harboring rare variants can be prioritized based on previously characterized roles in retinal development or function, interaction of the encoded protein with known IRD-associated proteins (Zeitz et al. 2005, 2006; Audo et al. 2009), in silico pathogenicity prediction scores (Siepel et al. 2005; Kircher et al. 2014; Schwarz et al. 2014; Ionita-Laza et al. 2016; Jaganathan et al. 2019), and thorough validation with model organisms to characterize the impact on retinal function (Bujakowska et al. 2015).

In this study we applied the above criteria to search for novel candidate gene in a large family with three affected siblings diagnosed with RCD. Two strong candidate genes were found to cosegregate with disease. *G protein nucleolar 3 (GNL3)* and *Phosphodiesterase 4D interacting protein (PDE4DIP)* both encode proteins that are involved with retinal development or known to interact with IRD-associated proteins (Kawashima et al. 2009; Overlack et al. 2011; Paridaen et al. 2011). Possible pathogenicity of the identified variants in both genes was studied in cell and zebrafish models; however, after exhaustive investigation, both candidate genes were excluded as the cause of disease. Ultimately the cause of disease was determined to be a difficult-to-detect structural variation in a known IRD gene, *PRPF31* (Vithana et al. 2001). In this case, partial penetrance displayed in the unaffected mother and sibling further complicated the genetic analysis because of a misleading inheritance pattern that was actually determined to be autosomal dominant with haploinsufficiency (Vithana et al. 2003; Abu-Safieh et al. 2006). Our study demonstrates the importance of a thorough validation of new candidate genes and the value of sequence data reanalysis.

RESULTS

A 30-yr-old female (OGI842-1649) was seen in the IRD clinic at Massachusetts Eye and Ear (MEE) with RCD. Family history revealed that five out of seven children in the family suffered from visual impairment, with no other history of retinal degeneration in the family (Fig. 1A). Subject OGI842-1649 had decreased visual acuity, restricted visual fields, and severely reduced cone responses in full-field electroretinograms (ERGs) (Table 1). Her fundus images showed characteristic signs of rod-cone degeneration including peripheral bone spicule pigmentation, vessel attenuation, and abnormal granularity in the macula retinal pigment epithelium (RPE) (Fig. 1B). Both parents were evaluated and showed no signs of retinal abnormalities, and full-field ERGs were within normal ranges (Table 1; Fig. 1B).

Molecular analysis was performed on the parents (OGI842-1653, OGI842-1831) and four siblings for whom DNA was available (OGI842-1649, OGI842-1650, OGI842-1651, and OGI842-1652). Potential causal variants obtained from exome sequencing were filtered

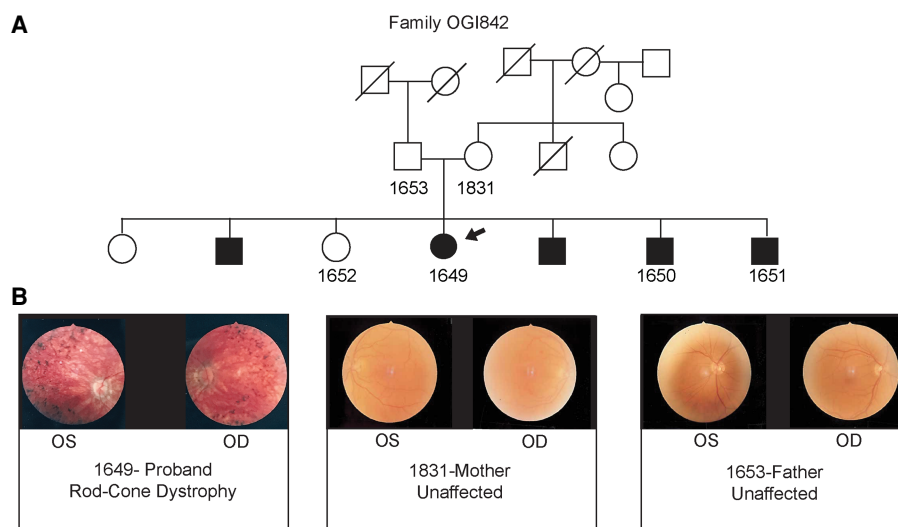


Figure 1. Pedigree and phenotypic details for family OGI842. (A) Multigenerational pedigree of OGI842 family. Affected are shown with darkened symbols, the proband is denoted with an arrow, and all subjects that were sequenced have a number designation. (B) Fundus images of the proband (OGI1649) age 33, unaffected 57-yr-old mother (OGI1831), and unaffected 58-yr-old father (OGI1653).

based on minor allele frequency (MAF) $\leq 0.1\%$. Whole-exome sequencing (WES) analysis identified rare biallelic variants in two candidate genes, *GNL3* with c.1187 + 3A > C and c.1568-8C > A splice region variants (Fig. 2A) and *PDE4DIP* with two missense variants (c.3868G > A, p.Glu1290Lys and c.4603G > A, p.Ala1535Thr) (Fig. 3A). Variants in both candidate genes were rare or absent in the gnomAD database and were selected for further analysis based on a combination of evolutionary conservation, aberrant splicing, and pathogenicity predictions (Table 2; Karczewski et al. 2020).

GNL3 encodes G protein nucleolar 3, also known as nucleostemin, which maintains cell proliferation and is necessary for the correct timing of cell cycle exit and differentiation (Tsai and McKay 2002). *GNL3* is expressed in retinal progenitor cells (Schmitt et al. 2009), and zebrafish *gnl3* mutants were shown to have smaller eyes and delayed retinal cell development (Paridaen et al. 2011). Therefore, we hypothesized that the two splice region variants c.1187 + 3A > C and c.1568-8C > A in *GNL3* may lead to retinal dysfunction. Both changes were absent in gnomAD and TOPMed. The c.1187 + 3A > C change, located in intron 11, was predicted to affect splicing by multiple splicing prediction software, whereas c.1568-8C > A in intron 14 had an elevated Eigen score (Ionita-Laza et al. 2016), and both were predicted to be disease causing by MutationTaster (Table 2; Schwarz et al. 2014). Both variants were studied by splicing assays in HEK293T cells. The splicing constructs spanned exons surrounding the studied variants with two controls: a wild type and an essential splice site control (Fig. 2B,C). Next-generation sequencing (NGS) analysis of the midgene transcripts revealed skipping of exon 11 and 12 in the c.1187 + 3A > C variant and essential splice site control (Fig. 2B). However, the second studied variant, c.1568-8C > A, had no effect on splicing (Fig. 2C). This variant was therefore considered to be nonpathogenic. In addition, knocking down *gnl3* with a splice blocking morpholino oligonucleotide (MO) in zebrafish did not show any morphological or functional effects on the eye or the retina (Supplemental Fig. S1). These findings conclusively dismissed *GNL3* as being the cause of disease in this family.

We therefore turned our attention toward the second candidate gene, *PDE4DIP*, whose product, myomegalin, is involved in cAMP-dependent signaling (Verde et al. 2001) and

Table 1. Clinical phenotypes of proband and parents

| Subject ID | Sex | Age at visit (yr) | Relationship | Status | Visual acuity (best corrected) | Visual field (normal \geq 120) | Fundus | Full-field ERG Normal values |
|-------------|-----|-------------------|--------------|------------|--------------------------------|----------------------------------|---|--|
| OG1842-1649 | F | 34 | Proband | RCD | OD: 20/30 OS: 20/30 | OD: 93.98 OS: 91.41 | Waxy pallor of optic disc, abnormal granularity of the RPE in the macula OU; peripheral bone spicule pigmentation, as well as attenuated vessels OU | 0.5-Hz amplitude: 350–700 μ V 30-Hz amplitude: 50–125 μ V 30-Hz implicit time: 25–32 msec |
| OG1842-1831 | F | 57 | Mother | Unaffected | OD:20/25+3 OS: 20/30 | Full | Optic disc, macula, vessels, and periphery all normal; minimal cortical lens opacities indicating mild cataracts; no evidence of RCD | OD: OS: 0.5-Hz amp: NA 2.70 μ V 30-Hz amp: 0.59 μ V 0.45 μ V 30-Hz time: 78 msec 78 msec |
| OG1842-1653 | M | 58 | Father | Unaffected | OD:20/20 OS: 20/200 | Full OD:100 OS: 114 | Optic disc, macula, and vessels are normal; nasal fundus slightly tigroid in periphery; no evidence of RCD | OD: OS: 0.5-Hz amp: 494 μ V No data 30-Hz amp: 41.2 μ V 65 μ V 30-Hz time: 31 msec 33 msec |
| | | | | | | | | OD: OS: 0.5-Hz amp: 317.6 μ V 470.6 μ V 30-Hz amp: 41.2 μ V 47.1 μ V 30-Hz time: 31 msec NA |

(ERG) Electroretinogram, (RCD) rod-cone dystrophy, (OU) both eyes, (OD) right eyes, (OS) left eye, (RPE) retinal pigment epithelium, (F) female, (M) male.

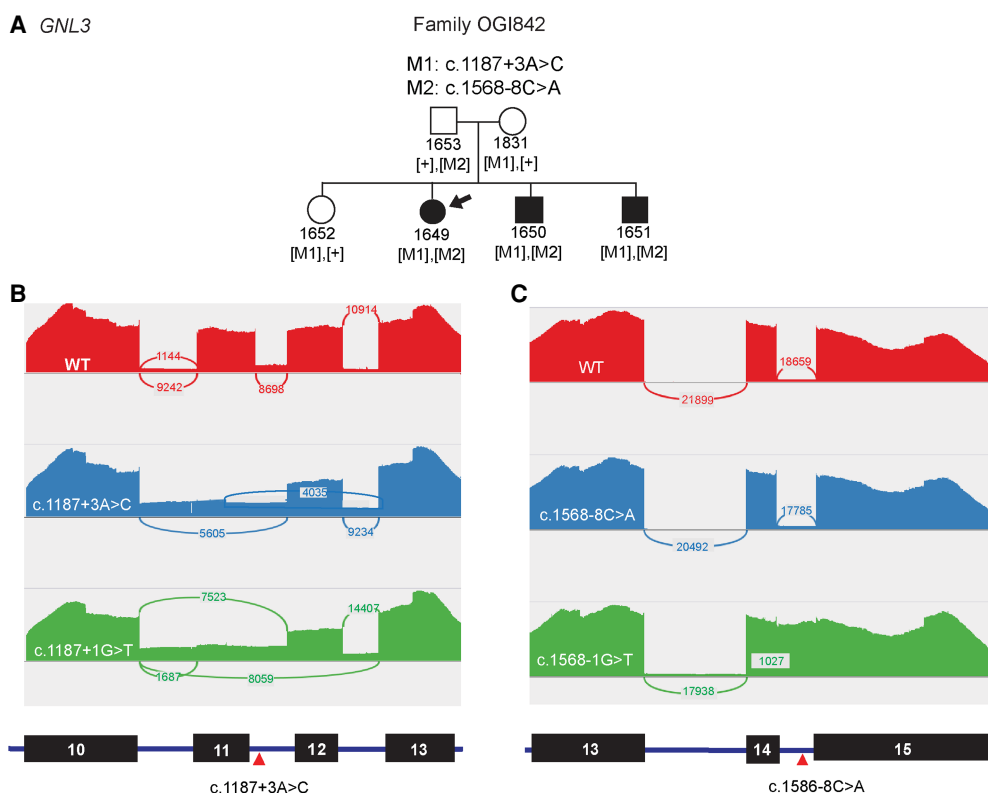


Figure 2. Investigating variants in *GNL3*, a candidate gene for inherited retinal degeneration (IRD). (A) Pedigree analysis confirms segregation of *GNL3* with disease; filled symbols represent affected individuals, empty symbols represent healthy individuals, circles are females, and squares are males. (B) Next-generation sequencing (NGS) analysis of mRNA splicing of the exon 10–13 minigene construct. Read coverage and exon junctions are represented by sashimi plots for the wild-type control (red), the c.1187 + 3A > C variant (blue), and the essential splice site control c.1187 + 1G > T (green). The corresponding minigene transcript model with the position of the mutation indicated with a red arrowhead is shown below. Exon 11 skipping (5605 junction reads) and intron 10 retention with partial exon 11 inclusion and exon 12 skipping (4035 reads) are the major effects of the c.1187 + 3A > C variant. Exon 11 skipping (7523 reads) and exon 11/12 skipping (8059 reads) are the major essential in the essential splice site control. Normalizing exon 11 splicing events to adjacent skipping of exon 11 occurs in 60% of transcripts (5605/9234 read ratio) as compared to wild type 9242/10,914, in which exon 12 skipping occurs in 43% (4035/9234 read ratio). (C) Sashimi plots generated from the amplicon sequencing on wild type (red), c.1568-8C > A (blue), and essential splice site mutation c.1568-1G > T (green) across regions of the minigene including exons 13–15. No difference is observed in the splicing pattern between the wild-type control and the c.1568-8C > A variant. Essential splice site control, c.1568-1G > T, showed complete intron 14 inclusion.

organization of centrosomal and Golgi-derived microtubules (Wang et al. 2014). Isoforms of myomegalin in the retina have been shown to interact with Sans, encoded by *USH1G*, Usher syndrome 1G (Overlack et al. 2011). Loss of *USH1G* causes congenital hearing loss and RCD (Mustapha et al. 2002), thus the implication of *PDE4DIP* playing a role in the Usher interactome made it a promising candidate gene for retinal degeneration (Weil et al. 2003). WES detected two missense variants in *PDE4DIP* (c.3868G > A, p.Glu1290Lys and c.4603G > A, p.Ala1535Thr; NM_001198834.3) that are rare in gnomAD and are highly conserved (Table 2; Fig. 3A,B; Karczewski et al. 2020).

Zebrafish studies were carried out to determine the effect of *pde4dip* MO knockdown on the retina (Fig. 3C,D; Supplemental Fig. S2). Even though no structural retinal abnormalities

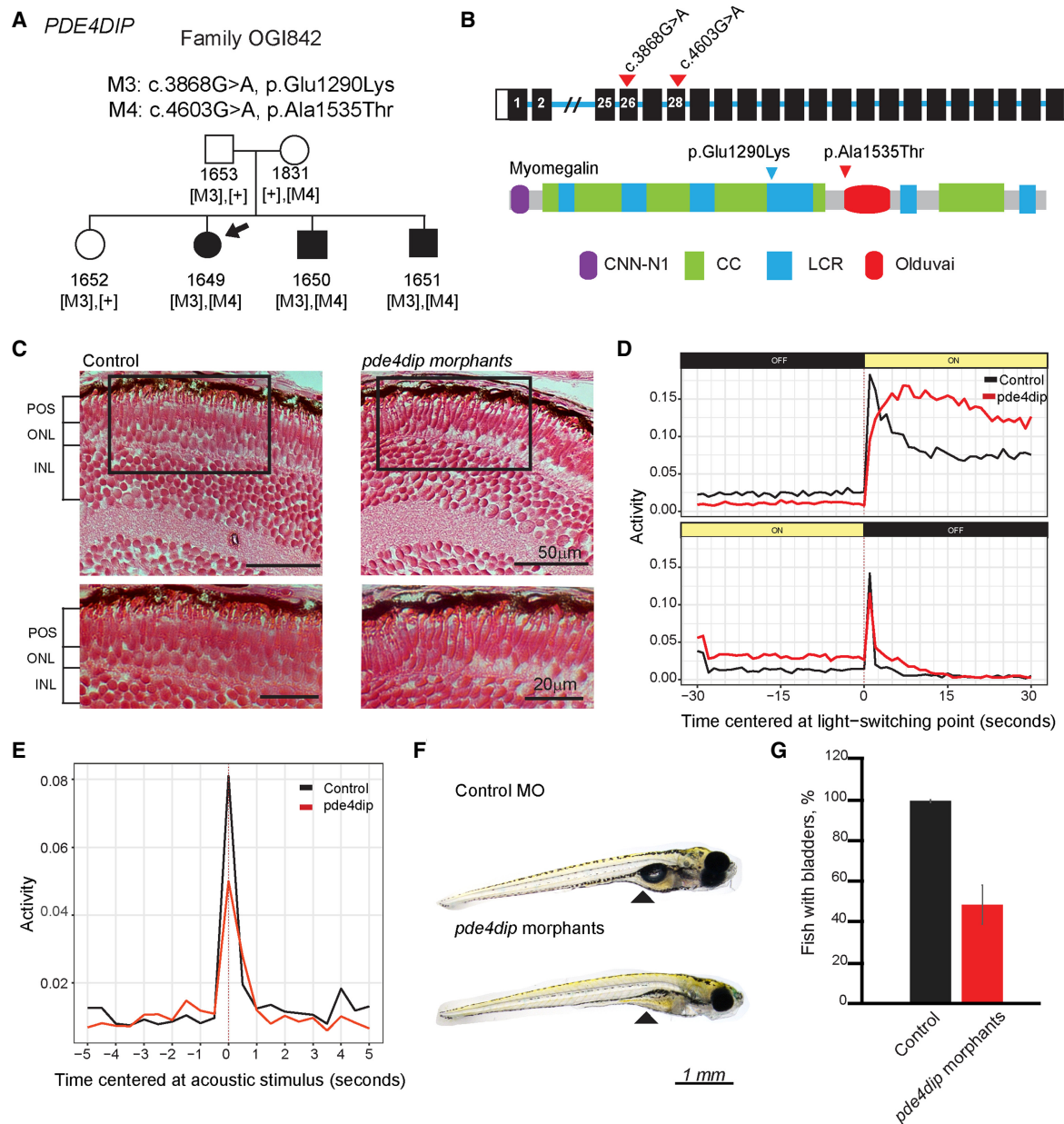


Figure 3. Investigating *PDE4DIP* as a candidate gene for inherited retinal degeneration (IRD). (A) Pedigree analysis confirming segregation of p.Glu1290Lys and p.Ala1535Thr missense variants. (B) Schematic of the *PDE4DIP* gene and the encoded protein (Myomegalin, PDB: MYOME_HUMAN (Q5VU43)) with mutations indicated (red arrowheads) in exons 26 and 28. (C) Retinal histology of *pde4dip* morphants at 5 d postfertilization (dpf), showing no observable differences in morphology as compared to controls. (D) Visual-motor response (VMR) assay showing a significant difference in response to light stimuli in *pde4dip* morphants (red, $n = 144$) and control MO (black, $n = 143$) (Tukey honestly significant difference [HSD], Light OFF $P = 2.73 \times 10^{-13}$, Light ON $P = 0.0136$). (E) Acoustically evoked behavior response (AEBR) assay showing decreased response in *pde4dip* morphants (red) compared to control fish (black) ($n = 144$, Tukey HSD, $P = 0.8996$) indicating general locomotor abnormalities. (F) Zebrafish analyzed at 5 dpf showing absence of gas bladders in *pde4dip* morphants. (G) Quantification of the gas bladder presence in *pde4dip* morphants (red) ($n = 134$, 54.48%) versus control fish (black) ($n = 134$, 98.51%), Fisher's exact test $P < 0.0001$.

Table 2. Variants identified in whole-exome sequencing

| Gene | cDNA change | Consequence | CADD | Mutation taster | Splice AI | gnomAD | Phast Con | Eigen | ClinVar | ACMG |
|----------------|-----------------|--------------------|------|-----------------|-----------|------------------------|-----------|-------|---------|---|
| <i>GNL3</i> | c.1187 + 3A > C | Exon skipping | 14 | Disease-causing | 0.75 | Absent | 0.999 | 18 | NR | LP (likely pathogenic), PVS1, PS3, PM2, PP1, PP3, BP5 |
| <i>GNL3</i> | c.1568-8C > A | NA | 7.4 | Disease-causing | 0.15 | Absent | 0.001 | 8.1 | NR | VUS (variant of uncertain significance), PM2, PM3, PP3, PP4, BS3, BP5 |
| <i>PDE4DIP</i> | c.3868G > A | p.Glu1290Lys | 32 | Disease-causing | 0.0 | 1.32×10^{-5} | 1.00 | 6.9 | NR | LB (likely benign), PM2, PP3, PP4, BS3, BP5 |
| <i>PDE4DIP</i> | c.4603G > A | p.Ala1535Thr | 23 | Polymorphism | 0.0 | 3.281×10^{-4} | 0.773 | 1.0 | NR | LB (likely benign), PM2, PP3, PP4, BS3, BP5 |
| <i>PRPF31</i> | c.73_166dup | p.Asp56Glyfs Ter33 | NA | Disease-causing | NA | Absent ^a | NA | NA | LP | P (pathogenic), PVS1, PM2, PP1, PP3, PP4 |

(CADD) Combined Annotation Dependent Depletion, (gnomAD) Genome Aggregation Database, (PhastCon) Phylogenetic Analysis with Space/Time models, (ACMG) American College of Medical Genetics and Genomics, (NR) not reported.

^aAbsent from both gnomAD and gnomAD-SV.

were observed (Fig. 3C), *pde4dip* morphants showed reduced function in the visual motor response (VMR) (Fig. 3D). To exclude the possibility that the reduced VMR response was a result of other developmental anomalies rather than retinal malfunction, we performed an acoustically evoked behavioral response (AEBR) assay. AEBR measures the motor response after an acoustic stimulus, providing a vision-independent control. In the AEBR experiment, *pde4dip* morphants had lowered startle response compared to control fish, indicating other developmental defects unrelated to vision were affecting motor response (Fig. 3E). Upon a closer inspection of the fish morphology, we realized that ~50% of the *pde4dip* morphants showed maldeveloped gas bladders, which indicates a general swimming impediment and explains reduced or lack of startle response upon visual or acoustic stimulation (Fig. 3F,G). Similar experiments repeated in CRISPR-Cas9 generated *pde4dip* mutant larvae also showed no retinal phenotype (Supplemental Figs. S3 and S4). Given this, we concluded that the *pde4dip* morphant phenotype is not specifically related to vision and that the loss of *pde4dip* in zebrafish and likely other organisms has no effect on retinal development and is unlikely the cause of disease in the studied family.

As both candidate genes were disproven, WES data was reanalyzed. Removing the inheritance and variant quality filters (variant quality score recalibration) (McKenna et al. 2010) led to the identification of a 94-nt tandem duplication within the first coding exon of Pre-mRNA Processing Factor 31, *PRPF31*, which is expressed in all tissues, including the retina (Lonsdale et al. 2013) (<https://www.gtportal.org/home/gene/PRPF31>). The *PRPF31* encoded protein, U4/U6 small nuclear ribonucleoprotein Prp31, facilitates protein-RNA interactions required for spliceosome assembly. The retina may be particularly sensitive to perturbations in splicing as mutations in splicing factors (Tanackovic et al. 2011), including *SNRNP200*, *PRPF3*, *PRPF8*, and *PRPF31* among others, are known to cause autosomal dominant rod-cone dystrophy (McKie et al. 2001; Vithana et al. 2001; Chakarova et al. 2002; Zhao et al. 2009). The duplication, c.73_166dup, leads to a frameshift that creates a stop codon, p.

Asp56GlyfsTer33 (Fig. 4A) most likely resulting in nonsense mediated decay of the transcript (Fig. 4B). Polymerase chain reaction (PCR) amplification of the region surrounding the duplication confirmed that all three affected family members (OGI842-1649, OGI842-1650, OGI842-1651) carry this variant, as well as the unaffected sibling (OGI842-1652) and the mother (OGI842-1831), indicating incomplete penetrance (Fig. 4C). Sanger sequencing confirmed mapping of the duplication to hg19: Chr 19:54,621,731–54,621,824 (Fig. 4D). The disease mechanism of *PRPF31* is known to be haploinsufficiency, and therefore the

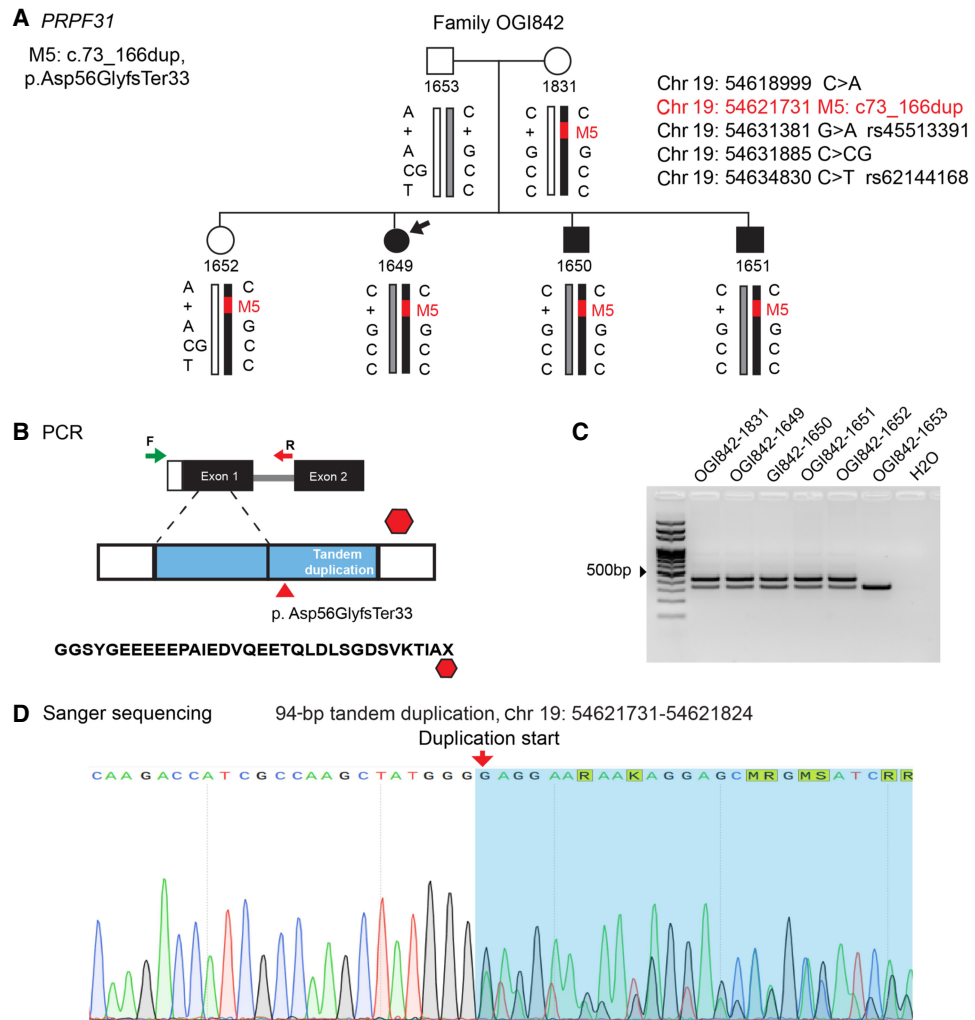


Figure 4. Validation of *PRPF31* duplication. (A) Familial segregation of the c.73_166dup, p.Asp56GlyfsTer33 variant (red bar) on maternal allele (black bar) revealing autosomal dominant inheritance pattern with partial penetrance. Segregation of the paternal wild-type allele among siblings with unaffected (white bar) and affected (gray bar). (B) A schematic diagram of the first two coding exons of *PRPF31* showing primers used to validate the proposed tandem duplication below. The altered amino acid sequence (p.Asp56GlyfsTer33) of the duplication results in the creation of a stop codon (red octagon). (C) Polymerase chain reaction (PCR) amplification of gDNA from all family members showing the heterozygous duplication (two bands) in all but the father (OGI842-1653). The lower band 335 bp is expected for wild-type allele, the upper band 429 bp is expected with the inclusion of the 94-bp duplication. (D) Chromatogram for Sanger sequencing shows start point for duplication with genomic location hg19 Chr 19:54621731-54621824.

uncovered heterozygous loss-of-function variant was determined to be the cause of disease in this family, with two asymptomatic mutation carriers. Partial penetrance, a known feature of *PRPF31*-associated RCD (Vithana et al. 2003; Rivolta et al. 2006), explains the initial assumption that disease inheritance in this pedigree was autosomal recessive. The inheritance of the wild-type allele was shown to determine disease penetrance (Vithana et al. 2003; Rivolta et al. 2006), which was also seen in the presented family, in which the unaffected sibling inherited a different wild-type allele from her father than the affected siblings (Fig. 4A).

DISCUSSION

Our study describes a search for the genetic cause of disease in an RCD family whose inheritance pattern appeared to be autosomal recessive with three affected members. WGS identified rare variants in two candidate genes that segregated with the disease phenotype and met the criteria determined in the outset of the study of being highly conserved, rare, or absent in genome aggregation databases, being predicted to be disease causing, and having relevant interactions with known IRD genes. The first candidate gene investigated, *GNL3*, also known as nucleostemin, belongs to a family of nucleolar GTP-binding proteins that includes members *GNL3L* and *GNL2*, which has been shown to be expressed in retinal precursors (Kawashima et al. 2009; Schmitt et al. 2009). Zebrafish models show both that *gnl2*^{-/-} and *gnl3*^{-/-} play a role in retinal neurogenesis with their loss leading to delayed retinal differentiation. Proteins coded by these genes have a partly redundant function with *gnl3*^{-/-} displaying a milder phenotype with transient abnormalities at early stages of development at 22 h postfertilization (hpf), which resolve at later time points (Paridaen et al. 2011). However, our results showed no phenotype associated with knockdown of *gnl3* using a splice blocking morpholino. Our attempts to use a translational blocking morpholino that would have arguably been a stronger knockdown and more closely comparable to the previous knockout model resulted in a “monster” phenotype and therefore could not be studied further. The lack of developmental phenotype in our *gnl3* morphants may also be due to the fact that we evaluated the morphant larvae at a later developmental stage, at 5 dpf rather than 22 hpf (Paridaen et al. 2011). Ultimately, the lack of phenotype in our zebrafish knockdown, as well as the absence of splicing aberrations in in vitro assays, led us to exclude *GNL3* as the cause of disease in this family. The second gene, *PDE4DIP*, encodes myomegalin, which has been shown to interact with SANS, an Usher interactome protein encoded by *USH1G* (Overlack et al. 2011). In the end, functional assays in zebrafish failed to demonstrate *PDE4DIP* impacted retinal function. Our results thus demonstrate the importance of not only the stringent selection criteria for candidate genes but also of rigorous functional validation to avoid falsely reporting new disease genes. Even though most of the new disease–gene associations demonstrate multiple levels of evidence for the pathogenicity of discovered variants, a recent study by Hanany and Sharon (2019) demonstrated a high false discovery rate within autosomal dominant IRD genes that was a result of mistakenly classified pathogenic variants. In our case, both genes appeared to be strong candidates and only functional analyses led to the exclusion of both candidate genes as the cause of disease.

Reanalysis of sequencing data led to the detection of a causative 94-bp tandem duplication (NM_015629.4:c.73_166dup (p.Asp56fs)), which creates a premature termination codon in *PRPF31*. The duplication was present in the unaffected mother and an unaffected sibling. The mother displayed no clinical manifestations of RCD even though she carried the mutation. The unaffected sibling not studied clinically, however, reported no symptoms. Additionally, she inherited an alternate wild-type allele compared to her affected siblings’ further supporting partial penetrance that obscured the autosomal dominant inheritance pattern. In addition, the 94-bp duplication is too large to be included in the

standard high-quality alignments and too small to be detected by read-depth copy-number variation (CNV) detection algorithms, such as gCNV (McKenna et al. 2010). This led to the *PRPF31* variant being excluded in the initial variant filtering, even though loss-of-function variants in *PRPF31* are a known cause of dominant RCD through haploinsufficiency (Abu-Safieh et al. 2006). Structural changes have increasingly been shown to contribute to retinal disease, with an estimated contribution of CNVs of up to 9% of IRD cases (Van Cauwenbergh et al. 2017; Ellingford et al. 2018; Zampaglione et al. 2020). Gene size has been shown to be the strongest predictor for genes enriched with structural variation followed by long interspersed nuclear elements (LINEs), long terminal repeats (LTRs), and segmental duplications (Van Schil et al. 2018). For example, *USH2A* is one of the largest IRD genes (800.5 kb, hg19 Chr 1:215,796,236–216,596,738), and a recent publication found potentially causal structural variants in 9% of an Usher syndrome cohort (Bonnet et al. 2016). *PRPF31*, however, is an outlier. It is a small gene (16.3 kb, hg19 Chr 19:54,621,731–54,621,824) that is not in proximity to regions prone to nonallelic homologous recombination (NAHR) (Bujakowska et al. 2016), yet likely causal CNVs account for a large number of patients with *PRPF31*-associated disease (Sullivan et al. 2006; Zampaglione et al. 2020). *PRPF31* does contain a large number of total repeats relative to its size including low copy repeats that flank unique sequences that lead to nonrecurrent CNVs (Carvalho and Lupski 2016), as well as LINEs and LTRs (Van Schil et al. 2018). In the present case, the location of the duplication is in a low-complexity region containing simple repeats, and the flanking sequences of the duplication contains a repeat (GCTATGGG) that may have facilitated DNA polymerase errors leading to the inclusion of the intervening region (Fig. 4D). The enrichment of genomic rearrangements combined with the complex inheritance pattern likely contributes to the underreporting of causal variants in *PRPF31*. Recent studies have shown diagnostic rates are improved by applying CNV analysis in an unbiased way in the initial analysis along with standard NGS pipelines, and this would allow for detection of causal CNVs in autosomal dominant genes such as *PRPF31* (Bonnet et al. 2016; Ellingford et al. 2018). The overall contribution of *PRPF31* mutations in IRD is likely underestimated and should be considered in apparent autosomal recessive pedigrees without a clear solution in a known IRD gene.

This case study highlights the importance of thorough functional characterization of new candidate genes and the value of reanalysis of NGS sequence data as false discovery of novel genes can obscure true genetic diagnosis and may prevent the use of appropriate gene-based therapies in affected patients.

METHODS

Ethical Guidelines

The study was approved by the institutional review board at the MEE, an affiliate of Mass General Brigham (MGB) healthcare system (Human Studies Committee MGB), and complied with the Health Information Portability and Accessibility Act (HIPAA). All aspects of the project adhered to the tenets of the Declaration of Helsinki. Informed consent was obtained from all individuals on whom genetic testing and further molecular evaluations were performed.

Clinical Evaluation

Ophthalmic evaluations were performed by clinicians experienced in inherited retinal degenerations at MEE. Visual acuity was measured using Snellen and Early Treatment of Diabetic Retinopathy Study (ETDRS) charts. Kinetic perimetry was performed using a Goldmann perimeter. Full-field ERG was performed using Burian Allen electrodes and

custom ERG system with previously described parameters (Reichel et al. 1989; Marmor et al. 2009).

Genetic Screening

DNA extracted from venous blood using the DNeasy Blood and Tissue Kit (QIAGEN) was used for all the sequencing reactions. WES was performed on OGI842–1649, OGI842–1651, OGI842–1653, and OGI842–1831, and data processing was performed by the Genomics Platform at the Broad Institute of MIT and Harvard with an Illumina exome capture (38 Mb target) and sequenced (150-bp paired reads) to cover >80% of targets at 20× and a mean target coverage of 100× (Supplemental Table S2). Exome sequencing data was processed through a pipeline based on Picard and mapping done using the BWA aligner to the human genome build 37 (hg19). The variant call sets were uploaded to variant analysis platform *seqr* (<http://seqr.broadinstitute.org>). Sanger sequencing was performed in all family members to validate potentially causal variants identified in WES including individuals who were not previously analyzed by WES (OGI842–1650 and OGI842–1652).

Splicing Assay

Variants selected for analysis with the midigene assay were evaluated for possible effects on splicing using both Alamut software (Alamut Visual; <http://www.interactive-biosoftware.com/alamut-visual/>) and Splice AI neural network (Jaganathan et al. 2019). Two constructs containing *GNL3* exons 10–13 including intronic regions and *GNL3* with exons 13–15 along with downstream 3′ regions, were amplified from patient’s genomic DNA (Pfu Ultra II polymerase, Agilent Technologies, primers listed in Supplemental Table S1). The PCR products were cloned into pENTR-TOPO/D (ThermoFisher) and verified by Sanger sequencing. Clones carrying essential splice-site mutations were created by site-directed mutagenesis (QuickChange II Site Directed mutagenesis kit, Agilent Technologies) on the wild-type constructs and verified by Sanger sequencing. Clones containing the desired sequences (wild-type, essential splice site, and variant to be studied) were subcloned into pCSGW2+ vector (Jamshidi et al. 2019) by Gateway cloning using LR clonase (Invitrogen).

pCSGW2+ *GNL3* constructs were transfected into HEK293 cells using 3 μg of total DNA and Lipofectamine reagent (Invitrogen) into six-well plates (Corning) seeded with 5×10^5 cells. Human embryonic kidney cells (HEK293T) were grown on Dulbecco’s Modified Eagle’s Media (Gibco) and 10% fetal bovine serum (Thermo Fisher) at 37°C and 5% CO₂. Total RNA was extracted from cells 72 h after transfection (RNAeasy mini kit, QIAGEN). cDNA was synthesized with Super Script II reverse transcriptase kit (Invitrogen) with 500 ng RNA input. Finally, PCR amplification using a primer directed toward the plasmid and a second primer specific to the insert containing flanking exons of the splice-site mutations (Supplemental Table S1) was performed followed by visualization by agarose gel electrophoresis and NGS (Illumina).

STAR (version 2.5.3a) aligner (Dobin et al. 2012) was used to generate an index of the human genome (GRCh37.75.dna.primary_assembly.fa) and to align the reads for the analysis of splicing patterns from amplicon sequencing. Integrative Genomics Viewer (IGV) (Robinson et al. 2011) was used to load the aligned sequences (BAM files) for data visualization with Sashimi plots.

Knockdown in Zebrafish

This study used an in-house cross of the AB and TL strain (source: ZIRC) for all experiments. Breeding and embryo maintenance were performed in accordance with MEE Zebrafish Core Facility standard procedures and IACUC-approved protocols. Embryos were injected at the one- to eight-cell stage, where each embryo received 2.3 nL of either 0.4 mM of the standard

control MO or 0.2 mM of each splice site blocking MO (Supplemental Table S1). cDNA was extracted from each condition and analyzed via PCR and Sanger sequencing to confirm the effect on splicing. Zebrafish larvae external phenotypes were evaluated at day 5. Histology was performed by sectioning zebrafish larvae in paraffin blocks and hematoxylin and eosin staining (SERI histology core, MGB).

To confirm morpholino results, CRISPR–Cas9 knockdown was performed targeting *pde4dip* exons 4 and 13. Zebrafish embryos were collected within 10 min of the beginning of breeding to ensure the one-cell stage of the embryos. Both sgRNA (targeting exons 4 and 13; Supplemental Table S1) and Cas9 protein (EnGen Spy Cas9, NEB) were coinjected into a cell cytoplasm of one-cell staged embryos. The mosaic F0 fish were kept for 5 d and analyzed functionally as morphant fish. Genomic DNA was extracted from the larvae after each assay and analyzed using NGS to observe cutting efficiency.

Visual-Motor Response and Acoustically Evoked Behavior Response

A combined VMR and AEBR assay was used to test the visual function and general motor function, respectively (Zeddies and Fay 2005; Emran et al. 2008; Faria et al. 2019). In brief, larvae at 5 dpf were tested using the ZebraLab system (ViewPoint Life Sciences). Larvae with body deformation or other severe external phenotypes were excluded. Individual larvae were placed in individual wells of a 96-well plate and placed in the ZebraLab system, which is isolated from outside vibration and light. In the AEBR test, larvae were adapted for 10 min before being challenged by three consecutive vibrations (200 Hz for 500 msec) with 5-min intervals under normal light illumination. In the VMR test, larvae were dark-adapted for 40 min before going through three consecutive trials of light onset and light offset periods that last for 30 min each (Emran et al. 2008). The light change (on or off) was abrupt and was not fading. The animal's motor response to the stimuli was recorded using infrared light and camera. All the functional tests were performed between 10 a.m. and 3 p.m.

Statistical Analysis of Zebrafish Functional Data

For the combined AEBR and VMR analysis, activity summarization and subsequent statistical analyses were performed using a customized analytical pipeline developed using R software (version 3.5.0; <http://www.r-project.org/>) building on previous analytical methods (Emran et al. 2008; Liu et al. 2015). The statistical analysis part of our analytical pipeline script is accessible in a GitHub repository: https://github.com/rongshisong/zebrafish_VMR_analysis. The differences between conditions and control in the mean activity level at the onset of the acoustic stimulation and during the first second after light change were tested using Tukey HSD with a *P*-value of 0.05 or greater considered significant. All experiments were done with at least *n* = 96 fish in each condition. Comparison of gas bladder presence was tested using Fisher's exact test.

ADDITIONAL INFORMATION

Data Deposition and Access

The causal variant identified in the present study has been deposited to ClinVar (<https://www.ncbi.nlm.nih.gov/clinvar/>) with accession number SCV001950339.

Ethics Statement

The study was approved by the institutional review board at the Massachusetts Eye and Ear (MEE), an affiliate of Mass General Brigham (MGB) healthcare system (Human Studies Committee MGB, Boston, MA, USA) and complied with the Health Information Portability

and Accessibility Act (HIPAA). All aspects of the project adhered to the tenets of the Declaration of Helsinki. Informed consent was obtained from all individuals on whom genetic testing and further molecular evaluations were performed.

Acknowledgments

The authors thank the patients and their family members for their participation in this study and the Ocular Genomics Institute Genomics Core members for their experimental assistance. The authors thank the Exome Aggregation Consortium, the Genome Aggregation Database (GnomAD), and the groups that provided exome variant data for comparison. A full list of contributing groups can be found at <http://exac.broadinstitute.org/about> and <http://gnomad.broadinstitute.org/about>.

Author Contributions

H.A.S. and A.L. performed experiments and contributed to the writing of the manuscript. R.B. assisted in animal model experiments. S.S.R. and S.M. provided data analysis. J.L.W. supported zebrafish data analysis and reviewed the manuscript. E.M.P. provided clinical data and reviewed the manuscript. E.A.P. contributed to the experimental design and reviewed the manuscript. K.R.C. analyzed sequencing data. K.M.B. guided the experimental design, provided variant analysis, and contributed to the writing of the manuscript.

Competing Interest Statement

The authors have declared no competing interest.

Referees

Peter N Robinson
Anonymous

Received August 3, 2021;
accepted in revised form
October 25, 2021.

Funding

This work was supported by grants from the National Eye Institute (R01EY026904 [K.M.B. and E.A.P.], R01EY012910 [E.A.P.], and P30EY014104 [MEEI core support]), the Foundation Fighting Blindness (EGI-GE-1218-0753-UCSD, K.M.B.), Research to Prevent Blindness (to K.M.B.), and the Curing Kids Foundation. Sequencing and analysis were provided by the Broad Institute of MIT and Harvard Center for Mendelian Genomics (Broad CMG) and were funded by the National Human Genome Research Institute, the National Eye Institute, and the National Heart, Lung, and Blood Institute grant UM1HG008900 and in part by National Human Genome Research Institute grant R01 HG009141.

REFERENCES

- Abu-Safieh L, Vithana EN, Mantel I, Holder GE, Pelosini L, Bird AC, Bhattacharya SS. 2006. A large deletion in the adRP gene *PRPF31*: evidence that haploinsufficiency is the cause of disease. *Mol Vis* **12**: 384–388.
- Arno G, Agrawal SA, Eblimit A, Bellingham J, Xu M, Wang F, Chakarova C, Parfitt DA, Lane A, Burgoyne T, et al. 2016. Mutations in *REEP6* cause autosomal-recessive retinitis pigmentosa. *Am J Hum Genet* **99**: 1305–1315. doi:10.1016/j.ajhg.2016.10.008
- Audo I, Kohl S, Leroy BP, Munier FL, Guillonneau X, Mohand-Saïd S, Bujakowska K, Nandrot EF, Lorenz B, Preising M, et al. 2009. *TRPM1* is mutated in patients with autosomal-recessive complete congenital stationary night blindness. *Am J Hum Genet* **85**: 720–729. doi:10.1016/j.ajhg.2009.10.013
- Bainbridge JWB, Smith AJ, Barker SS, Robbie S, Henderson R, Balaggan K, Viswanathan A, Holder GE, Stockman A, Tyler N, et al. 2008. Effect of gene therapy on visual function in Leber’s congenital amaurosis. *N Engl J Med* **358**: 2231–2239. doi:10.1056/NEJMoa0802268
- Bonnet C, Riahi Z, Chantot-Bastaraud S, Smagghe L, Letexier M, Marcaillou C, Lefèvre GM, Hardelin J-P, El-Amraoui A, Singh-Estivalet A, et al. 2016. An innovative strategy for the molecular diagnosis of Usher syndrome identifies causal biallelic mutations in 93% of European patients. *Eur J Hum Genet* **24**: 1730–1738. doi:10.1038/ejhg.2016.99
- Bujakowska KM, Zhang Q, Siemiatkowska AM, Liu Q, Place E, Falk MJ, Consugar M, Lancelot M-E, Antonio A, Lonjou C, et al. 2015. Mutations in *IFT172* cause isolated retinal degeneration and Bardet–Biedl syndrome. *Hum Mol Genet* **24**: 230–242. doi:10.1093/hmg/ddu441
- Bujakowska KM, Fernandez-Godino R, Place E, Consugar M, Navarro-Gomez D, White J, Bedoukian EC, Zhu X, Xie HM, Gai X, et al. 2016. Copy-number variation is an important contributor to the genetic causality of inherited retinal degenerations. *Genet Med* **19**: 643–651. doi:10.1038/gim.2016.158

- Carss KJ, Arno G, Erwood M, Stephens J, Sanchis-Juan A, Hull S, Megy K, Grozeva D, Dewhurst E, Malka S, et al. 2017. Comprehensive rare variant analysis via whole-genome sequencing to determine the molecular pathology of inherited retinal disease. *Am J Hum Genet* **100**: 75–90. doi:10.1016/j.ajhg.2016.12.003
- Carvalho CMB, Lupski JR. 2016. Mechanisms underlying structural variant formation in genomic disorders. *Nat Rev Genet* **17**: 224–238. doi:10.1038/nrg.2015.25
- Chakarova CF, Hims MM, Bolz H, Abu-Safieh L, Patel RJ, Papaioannou MG, Inglehearn CF, Keen TJ, Willis C, Moore AT, et al. 2002. Mutations in *HPRP3*, a third member of pre-mRNA splicing factor genes, implicated in autosomal dominant retinitis pigmentosa. *Hum Mol Genet* **11**: 87–92. doi:10.1093/hmg/11.1.87
- Consugar MB, Navarro-Gomez D, Place EM, Bujakowska KM, Sousa ME, Fonseca-Kelly ZD, Taub DG, Janessian M, Wang DY, Au ED, et al. 2014. Panel-based genetic diagnostic testing for inherited eye diseases is highly accurate and reproducible, and more sensitive for variant detection, than exome sequencing. *Genet Med* **17**: 253–261. doi:10.1038/gim.2014.172
- Dobin A, Davis CA, Schlesinger F, Drenkow J, Zaleski C, Jha S, Batut P, Chaisson M, Gingeras TR. 2012. STAR: ultrafast universal RNA-seq aligner. *Bioinformatics* **29**: 15–21. doi:10.1093/bioinformatics/bts635
- Ellingford JM, Horn B, Campbell C, Arno G, Barton S, Tate C, Bhaskar S, Sergouniotis PI, Taylor RL, Carss KJ, et al. 2018. Assessment of the incorporation of CNV surveillance into gene panel next-generation sequencing testing for inherited retinal diseases. *J Med Genet* **55**: 114–121. doi:10.1136/jmedgenet-2017-104791
- Emran F, Rihel J, Dowling JE. 2008. A behavioral assay to measure responsiveness of zebrafish to changes in light intensities. *J Vis Exp* **20**: 923. doi:10.3791/923
- Faria M, Prats E, Novoa-Luna KA, Bedrossiantz J, Gómez-Canela C, Gómez-Oliván LM, Raldúa D. 2019. Development of a vibrational startle response assay for screening environmental pollutants and drugs impairing predator avoidance. *Sci Total Environ* **650**: 87–96. doi:10.1016/j.scitotenv.2018.08.421
- Haim M. 2002. Epidemiology of retinitis pigmentosa in Denmark. *Acta Ophthalmol Scand Suppl* **233**: 1–34. doi:10.1046/j.1395-3907.2002.00001.x
- Hanany M, Sharon D. 2019. Allele frequency analysis of variants reported to cause autosomal dominant inherited retinal diseases question the involvement of 19% of genes and 10% of reported pathogenic variants. *J Med Genet* **56**: 536–542. doi:10.1136/jmedgenet-2018-105971
- Ionita-Laza I, McCallum K, Xu B, Buxbaum JD. 2016. A spectral approach integrating functional genomic annotations for coding and noncoding variants. *Nat Genet* **48**: 214–220. doi:10.1038/ng.3477
- Jaganathan K, Kyriazopoulou Panagiotopoulou S, McRae JF, Darbandi SF, Knowles D, Li YI, Kosmicki JA, Arbelaez J, Cui W, Schwartz GB, et al. 2019. Predicting splicing from primary sequence with deep learning. *Cell* **176**: 535–548.e24. doi:10.1016/j.cell.2018.12.015
- Jamshidi F, Place EM, Mehrotra S, Navarro-Gomez D, Maher M, Branham KE, Valkanas E, Cherry TJ, Lek M, MacArthur D, et al. 2019. Contribution of noncoding pathogenic variants to RPGRIP1-mediated inherited retinal degeneration. *Genet Med* **21**: 694–704. doi:10.1038/s41436-018-0104-7
- Karczewski KJ, Francioli LC, Tiao G, Cummings BB, Alföldi J, Wang Q, Collins RL, Laricchia KM, Ganna A, Birnbaum DP, et al. 2020. The mutational constraint spectrum quantified from variation in 141,456 humans. *Nature* **581**: 434–443.
- Kawashima M, Kawakita T, Yoshida S, Shimmura S, Tsubota K. 2009. Nucleostemin as a possible progenitor marker of corneal epithelial cells. *Mol Vis* **15**: 1162–1168.
- Khateb S, Kowalewski B, Bedoni N, Damme M, Pollack N, Saada A, Obolensky A, Ben-Yosef T, Gross M, Dierks T, et al. 2018. A homozygous founder missense variant in arylsulfatase G abolishes its enzymatic activity causing atypical Usher syndrome in humans. *Genet Med* **20**: 1004–1012. doi:10.1038/gim.2017.227
- Kircher M, Witten DM, Jain P, O’Roak BJ, Cooper GM. 2014. A general framework for estimating the relative pathogenicity of human genetic variants. *Nat Genet* **46**: 310–315. doi:10.1038/ng.2892
- Li L, Jiao X, D’Atri I, Ono F, Nelson R, Chan CC, Nakaya N, Ma Z, Ma Y, Cai X, et al. 2018. Mutation in the intracellular chloride channel CLCC1 associated with autosomal recessive retinitis pigmentosa. *PLoS Genet* **14**: e1007504. doi:10.1371/journal.pgen.1007504
- Liu Y, Carmer R, Zhang G, Venkatraman P, Brown SA, Pang C-P, Zhang M, Ma P, Leung YF. 2015. Statistical analysis of zebrafish locomotor response. *PLoS ONE* **10**: e0139521. doi:10.1371/journal.pone.0139521
- Lonsdale J, Thomas J, Salvatore M, Phillips R, Lo E, Shad S, Hasz R, Walters G, Garcia F, Young N, et al. 2013. The genotype-tissue expression (GTEx) project. *Nat Genet* **45**: 580–585. doi:10.1038/ng.2653
- MacLaren RE, Groppe M, Barnard AR, Cottrill CL, Tolmachova T, Seymour L, Clark KR, During MJ, Cremers FPM, Black GCM, et al. 2014. Retinal gene therapy in patients with choroideremia: initial findings from a phase 1/2 clinical trial. *Lancet* **383**: 1129–1137. doi:10.1016/S0140-6736(13)62117-0
- Maguire AM, Simonelli F, Pierce EA, Pugh EN, Mingozzi F, Bennicelli J, Banfi S, Marshall KA, Testa F, Surace EM, et al. 2008. Safety and efficacy of gene transfer for leber’s congenital amaurosis. *N Engl J Med* **358**: 2240–2248. doi:10.1056/NEJMoa0802315

- Marmor MF, Fulton AB, Holder GE, Miyake Y, Brigell M, Bach M. 2009. ISCEV standard for full-field clinical electroretinography (2008 update). *Doc Ophthalmol* **118**: 69–77. doi:10.1007/s10633-008-9155-4
- McKenna A, Hanna M, Banks E, Sivachenko A, Cibulskis K, Kernysky A, Garimella K, Altshuler D, Gabriel S, Daly M, et al. 2010. The Genome Analysis Toolkit: a MapReduce framework for analyzing next-generation DNA sequencing data. *Genome Res* **20**: 1297–1303. doi:10.1101/gr.107524.110
- McKie AB, McHale JC, Keen TJ, Tarttelin EE, Goliath R, van Lith-Verhoeven JJC, Greenberg J, Ramesar RS, Hoyng CB, Cremers FPM, et al. 2001. Mutations in the pre-mRNA splicing factor gene *PRPC8* in autosomal dominant retinitis pigmentosa (RP13). *Hum Mol Genet* **10**: 1555–1562. doi:10.1093/hmg/10.15.1555
- Mustapha M, Chouery E, Torchard-Pagnez D, Nouaille S, Khrais A, Sayegh FN, Mégarbané A, Loiselet J, Lathrop M, Petit C, et al. 2002. A novel locus for Usher syndrome type I, USH1G, maps to Chromosome 17q24–25. *Hum Genet* **110**: 348–350. doi:10.1007/s00439-002-0690-x
- Overlack N, Kilic D, Bauß K, Märker T, Kremer H, van Wijk E, Wolfrum U. 2011. Direct interaction of the Usher syndrome 1G protein SANS and myomegalin in the retina. *Biochim Biophys Acta Mol Cell Res* **1813**: 1883–1892. doi:10.1016/j.bbamcr.2011.05.015
- Paridaen JTML, Janson E, Utami KH, Pereboom TC, Essers PB, van Rooijen C, Zivkovic D, MacInnes AW. 2011. The nucleolar GTP-binding proteins Gnl2 and nucleostemin are required for retinal neurogenesis in developing zebrafish. *Dev Biol* **355**: 286–301. doi:10.1016/j.ydbio.2011.04.028
- Reichel E, Bruce AM, Sandberg MA, Berson EL. 1989. An electroretinographic and molecular genetic study of X-linked cone degeneration. *Am J Ophthalmol* **108**: 540–547. doi:10.1016/0002-9394(89)90431-5
- Rivolta C, McGee TL, Rio Frio T, Jensen RV, Berson EL, Dryja TP. 2006. Variation in retinitis pigmentosa-11 (*PRPF31* or *RP11*) gene expression between symptomatic and asymptomatic patients with dominant *RP11* mutations. *Hum Mutat* **27**: 644–653. doi:10.1002/humu.20325
- Robinson JT, Thorvaldsdóttir H, Winckler W, Guttman M, Lander ES, Getz G, Mesirov JP. 2011. Integrative genomics viewer. *Nat Biotechnol* **29**: 24–26. doi:10.1038/nbt.1754
- Schmitt S, Aftab U, Jiang C, Redenti S, Klassen H, Miljan E, Sinden J, Young M. 2009. Molecular characterization of human retinal progenitor cells. *Invest Ophthalmol Vis Sci* **50**: 5901–5908. doi:10.1167/iovs.08-3067
- Schwarz JM, Cooper DN, Schuelke M, Seelow D. 2014. MutationTaster2: mutation prediction for the deep-sequencing age. *Nat Methods* **11**: 361–362. doi:10.1038/nmeth.2890
- Siepel A, Bejerano G, Pedersen JS, Hinrichs AS, Hou M, Rosenbloom K, Clawson H, Spieth J, Hillier LW, Richards S, et al. 2005. Evolutionarily conserved elements in vertebrate, insect, worm, and yeast genomes. *Genome Res* **15**: 1034–1050. doi:10.1101/gr.3715005
- Sullivan LS, Bowne SJ, Seaman CR, Blanton SH, Lewis RA, Heckenlively JR, Birch DG, Hughbanks-Wheaton D, Daiger SP. 2006. Genomic rearrangements of the *PRPF31* gene account for 2.5% of autosomal dominant retinitis pigmentosa. *Invest Ophthalmol Vis Sci* **47**: 4579–4588. doi:10.1167/iovs.06-0440
- Tanackovic G, Ransijn A, Thibault P, Abou Elela S, Klinck R, Berson EL, Chabot B, Rivolta C. 2011. *PRPF* mutations are associated with generalized defects in spliceosome formation and pre-mRNA splicing in patients with retinitis pigmentosa. *Hum Mol Genet* **20**: 2116–2130. doi:10.1093/hmg/ddr094
- Tsai RY, McKay RD. 2002. A nucleolar mechanism controlling cell proliferation in stem cells and cancer cells. *Genes Dev* **16**: 2991–3003. doi:10.1101/gad.55671
- Van Cauwenbergh C, Van Schil K, Cannoodt R, Bauwens M, Van Laethem T, De Jaegere S, Steyaert W, Sante T, Menten B, Leroy BP, et al. 2017. arrEYE: a customized platform for high-resolution copy number analysis of coding and noncoding regions of known and candidate retinal dystrophy genes and retinal noncoding RNAs. *Genet Med* **19**: 457–466. doi:10.1038/gim.2016.119
- Van Schil K, Naessens S, Van de Sompele S, Carron M, Aslanidis A, Van Cauwenbergh C, Mayer AK, Van Heetvelde M, Bauwens M, Verdin H, et al. 2018. Mapping the genomic landscape of inherited retinal disease genes prioritizes genes prone to coding and noncoding copy-number variations. *Genet Med* **20**: 202–213. doi:10.1038/gim.2017.97
- Verde I, Pahlke G, Salanova M, Zhang G, Wang S, Coletti D, Onuffer J, Jin SLC, Conti M. 2001. Myomegalin is a novel protein of the golgi/centrosome that interacts with a cyclic nucleotide phosphodiesterase. *J Biol Chem* **276**: 11189–11198. doi:10.1074/jbc.M006546200
- Vithana EN, Abu-Safieh L, Allen MJ, Carey A, Papaioannou M, Chakarova C, Al-Magthteh M, Ebenezer ND, Willis C, Moore AT, et al. 2001. A human homolog of yeast pre-mRNA splicing gene, *PRP31*, underlies autosomal dominant retinitis pigmentosa on Chromosome 19q13.4 (*RP11*). *Mol Cell* **8**: 375–381. doi:10.1016/S1097-2765(01)00305-7
- Vithana EN, Abu-Safieh L, Pelosini L, Winchester E, Hornan D, Bird AC, Hunt DM, Bustin SA, Bhattacharya SS. 2003. Expression of *PRPF31* mRNA in patients with autosomal dominant retinitis pigmentosa: a molecular clue for incomplete penetrance? *Invest Ophthalmol Vis Sci* **44**: 4204–4209. doi:10.1167/iovs.03-0253
- Wang Z, Zhang C, Qi RZ. 2014. A novel myomegalin isoform functions in Golgi microtubule organization and ER–Golgi transport. *J Cell Sci* **127**: 4904–4917. doi:10.1242/jcs.131045
- Weil D, El-Amraoui A, Masmoudi S, Mustapha M, Kikkawa Y, Lainé S, Delmaghani S, Adato A, Nadifi S, Zina ZB, et al. 2003. Usher syndrome type I G (*USH1G*) is caused by mutations in the gene encoding SANS, a protein

- that associates with the USH1C protein, harmonin. *Hum Mol Genet* **12**: 463–471. doi:10.1093/hmg/ddg051
- Xu M, Yamada T, Sun Z, Eblimit A, Lopez I, Wang F, Manya H, Xu S, Zhao L, Li Y, et al. 2016. Mutations in *POMGNT1* cause non-syndromic retinitis pigmentosa. *Hum Mol Genet* **25**: 1479–1488. doi:10.1093/hmg/ddw022
- Zampaglione E, Kinde B, Place EM, Navarro-Gomez D, Maher M, Jamshidi F, Nassiri S, Mazzone JA, Finn C, Schlegel D, et al. 2020. Copy-number variation contributes 9% of pathogenicity in the inherited retinal degenerations. *Genet Med* **22**: 1079–1087. doi:10.1038/s41436-020-0759-8
- Zeddies DG, Fay RR. 2005. Development of the acoustically evoked behavioral response in zebrafish to pure tones. *J Exp Biol* **208**: 1363–1372. doi:10.1242/jeb.01534
- Zeitz C, van Genderen M, Neidhardt J, Luhmann UFO, Hoeben F, Forster U, Wycisk K, Mátyás GB, Hoyng CB, Riemsdag F, et al. 2005. Mutations in *GRM6* cause autosomal recessive congenital stationary night blindness with a distinctive scotopic 15-Hz flicker electroretinogram. *Invest Ophthalmol Vis Sci* **46**: 4328–4335. doi:10.1167/iovs.05-0526
- Zeitz C, Kloeckener-Gruissem B, Forster U, Kohl S, Magyar I, Wissinger B, Mátyás G, Borruat F-X, Schorderet DF, Zrenner E, et al. 2006. Mutations in *CABP4*, the gene encoding the Ca²⁺-binding protein 4, cause autosomal recessive night blindness. *Am J Hum Genet* **79**: 657–667. doi:10.1086/508067
- Zhao C, Bellur DL, Lu S, Zhao F, Grassi MA, Bowne SJ, Sullivan LS, Daiger SP, Chen LJ, Pang CP, et al. 2009. Autosomal-dominant retinitis pigmentosa caused by a mutation in *SNRNP200*, a gene required for unwinding of U4/U6 snRNAs. *Am J Hum Genet* **85**: 617–627. doi:10.1016/j.ajhg.2009.09.020
- Zhou Y, Li S, Huang L, Yang Y, Zhang L, Yang M, Liu W, Ramasamy K, Jiang Z, Sundaresan P, et al. 2018. A splicing mutation in aryl hydrocarbon receptor associated with retinitis pigmentosa. *Hum Mol Genet* **27**: 2563–2572. doi:10.1093/hmg/ddy165